Coupling between surface ozone and leaf area index in a chemical transport model: Strength of feedback and implications for ozone air quality and vegetation health

Shan S. Zhou[1], Amos P. K. Tai[1,2], Shihan Sun[1], Mehliyar Sadiq[1], Colette L. Heald[3], Jeffrey A. Geddes[4]

5 [1] Earth System Science Programme and Graduate Division of Earth and Atmospheric Sciences, Faculty of Science, The Chinese University of Hong Kong, Sha Tin, Hong Kong
[2] Partner State Key Laboratory of Agrobiotechnology and Institute of Environment, Energy and Sustainability, The Chinese University of Hong Kong, Sha Tin, Hong Kong
[3] Department of Civil and Environmental Engineering and Department of Earth, Atmospheric and Planetary Sciences,
10 Massachusetts Institute of Technology, Cambridge, USA
[4] Department of Earth and Environment, Boston University, Boston, USA

Correspondence to: Amos P. K. Tai (amostai@cuhk.edu.hk)

Abstract. Tropospheric ozone is a significant air pollutant with substantial harm on vegetation, but is also strongly dependent on various vegetation-mediated processes. The interdependence between ozone and vegetation may constitute feedback
15 mechanisms that can alter ozone concentration itself but have not been considered in most studies to date. In this study we examine the importance of biogeochemical coupling between surface ozone and leaf area index (LAI) in shaping ozone air quality and foliage density. We first implement an empirical scheme for ozone damage on vegetation in the Community Land Model (CLM), and simulate the steady-state responses of LAI to long-term exposure to a range of prescribed ozone levels (from 0 ppb to 100 ppb). We find that most plant functional types (PFTs) suffer a substantial decline in LAI as ozone level
20 increases. Based on the CLM-simulated results, we develop and implement in the GEOS-Chem chemical transport model a parameterization that correlates the fractional changes in monthly LAI to local mean ozone levels. By dynamically forcing LAI to respond to ozone concentrations on a monthly timescale, the model simulates ozone-vegetation coupling synchronously via biogeochemical processes including biogenic volatile organic compound (VOC) emissions and dry deposition. We find that ozone-induced damage on LAI can lead to an ozone feedback of -1.8 ppb to $+3$ ppb in northern summer, with a
25 corresponding ozone feedback factor of -0.1 to $+0.6$. Significantly higher simulated ozone due to strong positive ozone-LAI feedback is found in most tropical forests, mainly due to the ozone-induced reductions in LAI and dry deposition velocity, whereas reduced isoprene emission plays a lesser role in these low-NO_x environments. In high-NO_x regions such as eastern US, Europe and China, however, the feedback effect is much weaker and even negative in some regions, reflecting the compensating effects of reduced dry deposition and reduced isoprene emission (which leads to lower ozone in the high-NO_x
30 regime). In remote, low-LAI regions including most of the Southern Hemisphere, the ozone feedback is generally slightly negative, likely due to reduced transport of NO_x-VOC reaction products that serve as NO_x reservoirs. This study represents the

first step to account for dynamic ozone-vegetation coupling in a chemical transport model with important ramifications for more realistic assessment of ozone air quality and ecosystem health.

1 Introduction

Tropospheric ozone (O_3) is an important greenhouse gas with an estimated radiative forcing of 0.40 ± 0.20 W m^{-2}
5 [*IPCC*, 2013]. It is also a significant air pollutant shown to have harmful effects on both human health and vegetation, including crops [*Anenberg et al.*, 2010; *Ainsworth et al.*, 2012]. Tropospheric ozone is primarily produced from the photochemical oxidation of various precursor species including carbon monoxide (CO), methane (CH_4) and volatile organic compounds (VOCs) by hydroxyl radicals (OH) in the presence of nitrogen oxides ($NO_x \equiv NO + NO_2$). Most of the precursors have large anthropogenic sources from industrial and agricultural activities, and tropospheric ozone concentrations have been increasing
10 since the industrial revolution. The earliest surface ozone observations recorded at L'Observatoire de Montsouris near Paris showed an annual mean ozone concentration of 11 ppb for the 1876-1910 period in Europe [*Volz and Kley*, 1988]. Ozone concentrations displayed a significant upward trend at northern midlatitudes during 1970s-1980s, and then a flattening or even declining trend depending on the region in the last two decades [*Oltmans et al.*, 2013]. As anthropogenic emissions are expected to decrease in many countries due to more stringent regulation [van Vuuren et al., 2011], other factors such as climate,
15 land surface and vegetation changes will likely have increasingly important roles shaping future ozone levels [e.g., Tai et al., 2013; Wong et al., 2017]. In this study, we in particular examine the possible roles of two-way interactions between ozone and vegetation in modulating surface ozone air quality using an offline-coupled land-atmosphere modeling framework.

Vegetation can significantly influence both the sources and sinks of tropospheric ozone. Globally, precursors from natural sources play an important role in ozone formation. They include such gases as NO_x, CH_4 and various non-methane
20 VOCs (NMVOCs) emitted by land vegetation and soil microbes. Isoprene (C_5H_8), which is the most abundant biogenic NMVOCs species emitted by vegetation [*Guenther et al.*, 2006], is a major ozone precursor in high-NO_x environments, but can consume ozone by direct ozonolysis or reduce ozone by sequestering NO_x via the formation of isoprene nitrate and peroxyacetyl nitrate (PAN) in low-NO_x environments [*Horowitz et al.*, 2007; *Hollaway et al.*, 2017]. On the other hand, the major sinks for surface ozone include the in-situ chemical reactions with water vapor (H_2O), hydrogen peroxide (HO_2) and
25 OH [*Wild*, 2007], and the dry deposition of ozone onto vegetation mainly through leaf stomatal uptake [*Wang et al.*, 1998]. Vegetation can therefore influence surface ozone via biogenic VOC emissions and dry deposition as well as transpiration, which modulates boundary-layer mixing, temperature, water vapor content, and thus the dilution and chemical loss of ozone.

Surface ozone can in turn influence vegetation. The stomatal uptake of ozone has been shown to damage plants and reduce photosynthetic CO_2 assimilation at the leaf level, which may in turn reduce leaf area index (LAI), gross primary
30 productivity (GPP), and crop yield [*Karnosky et al.*, 2007; *Ainsworth et al.*, 2012]. *Yue and Unger* [2014] developed a terrestrial ecosystem model to assess the damage of surface ozone on gross primary productivity (GPP) throughout the US, and found that GPP is reduced by 4-8% on average in the eastern US in the growing season due to exposure to year-2005 ozone levels.

Another study also found that global GPP and transpiration are reduced by 11% and 2.2%, respectively, under exposure to present-day ozone concentrations, with the greatest damage (20–25% for GPP, 15–20% for transpiration) happening at northern midlatitudes [*Lombardozzi et al.*, 2015]. As vegetation variables such as stomatal resistance, LAI, and plant functional type (PFT) distribution all play important roles shaping surface ozone, dynamic changes in these variables following ozone

5 damage may thus induce a cascade of feedbacks that ultimately affect ozone itself. The impact of such ozone-vegetation coupling on ozone air quality has only recently been examined by *Sadiq et al.* [2017], who found that by implementing synchronous ozone-vegetation coupling in the Community Earth System Model (CESM), simulated present-day surface ozone concentrations can be higher by 4–6 ppb over North America, Europe and China. Roughly half of such an enhancement is caused by reduced ozone dry deposition following increased stomatal resistance, and the rest mostly arises from reduced

10 transpiration that leads to higher vegetation temperature and thus isoprene emission. They suggested that a major challenge in diagnosing the various feedback pathways is the high uncertainty associated with the temperature and precipitation responses to transpiration changes.

Previous modeling studies of ozone damage on vegetation usually used prescribed structural variables (e.g., LAI, canopy height) derived from satellites and land surveys as fixed parameters in their vegetation simulations [e.g., *Sitch et al.*,

15 2007; *Lombardozzi et al.*, 2015]. Some studies have considered the long-term decline in growth and LAI following ozone damage on GPP, which further limits GPP itself [*Yue and Unger*, 2015] and can lead to a biogeochemical feedback effect on air quality due to the importance of LAI in modulating surface ozone and hydrometeorology [*Sadiq et al.*, 2017]. Observation-based, prescribed LAI may be adequate for present-day or short-term simulations of vegetation and climate, but with ozone-vegetation interaction as well as other drivers such as warming and rising CO_2, historical and future foliage properties may be

20 significantly different from those in the present day. Prognostic LAI simulated dynamically by biogeochemical models may therefore be required to enable more realistic simulations especially for multidecadal and century-long historical simulations or future projections under rather different climate scenarios. Furthermore, while ozone concentration generally responds and equilibrates with any changes in the terrestrial boundary conditions over relatively short timescales (hours to weeks), the responses of vegetation to ozone exposure are usually slower and may require months to years to fully take effect due to the

25 cumulative nature of ozone damage [*Lombardozzi et al.*, 2012]. It is essential to examine different timescales of ozone-vegetation coupling, and decide accordingly the most suitable and computationally efficient model coupling approach to adequately capture the interactive effects.

In this study, we use a standalone land surface model (LSM) with active biogeochemical cycles driven by prescribed meteorological inputs and ozone concentrations to examine the long-term evolution of LAI in response to different levels of

30 ozone exposure. Based on the simulated ozone-LAI relationships, we develop a simplified parameterization scheme for synchronous coupling between ozone and LAI on a monthly timescale for computationally efficient use in air quality assessment by a chemical transport model (CTM). We also investigate the effect of asynchronous coupling by performing a series of offline-coupled LSM-CTM model experiments. By comparing simulated ozone concentrations from CTM simulations with vs. without ozone-induced damage on LAI, we quantify the "ozone feedback" that results from ozone-

vegetation coupling, and examine the possible pathways contributing to the feedback. This effort not only allows ozone-vegetation coupling to be considered dynamically online within a regional climate or air quality model without the complication arising from hydrometeorological changes and feedbacks, but also renders the incorporation of ozone-induced biogeochemical feedbacks and air quality-ecosystem coevolution more computationally affordable in regional climate and air

5   quality models.

2 Model description and simulations

2.1 Basic description for Community Land Model

In this study, we simulate ozone damage on vegetation using the Community Land Model (CLM) version 4.5,

10   embedded within the Community Earth System Model (CESM) version 1.2.2 forced by prescribed atmospheric data at a resolution of 1.9° latitude by 2.5° longitude. This version not only updates important canopy processes including canopy radiation and upscaling of leaf processes from previous versions, but also improves the stability of the iterative solution in the computation of photosynthesis and stomatal conductance [*Sun et al.*, 2012]. We use the "BGC mode" with active biogeochemistry [*Oleson et al.*, 2013], which dynamically simulates ecosystem structural variables (LAI and canopy height)

15   based on post-photosynthesis carbon allocation. When evaluated against regional observations, this version of CLM typically captures the spatial variability of gross primary production (GPP) and LAI well, albeit with different signs and degrees of region-specific biases including a general overestimation in both variables in humid, highly productive regions [e.g., *Wang et al.*, 2015; *Sakalli et al.*, 2017].

CLM4.5 uses the Ball-Berry stomatal conductance model [*Ball et al.*, 1987] described by *Collatz et al.* [1991] to

20   simulate leaf stomatal conductance (g_s) as

$$g_s = \frac{1}{r_s} = m \frac{A_n}{c_s} h_s P_{\text{atm}} + b \tag{1}$$

where r_s is the leaf stomatal resistance (s m^2 μmol^{-1}), m is a PFT-dependent parameter ($m = 9$ for C$_3$ plants and $m = 4$ for C$_4$ plants), A_n is the leaf net photosynthesis rate (μmol CO$_2$ m^{-2} s^{-1}), c_s is the CO$_2$ partial pressure at the leaf surface (Pa), $h_s = e_s/e_i$ is the leaf surface fractional humidity with e_s being the vapor pressure (Pa) at the leaf surface and e_i being the saturation vapor

25   pressure (Pa) at leaf temperature, P_{atm} is the atmospheric pressure (Pa), and b is the minimum stomatal conductance (μmol m^{-2} s^{-1}) ($b = 10000$ for C$_3$ plants and $b = 40000$ for C$_4$ plants) when there is no net photosynthesis.

The rate of net photosynthesis, A_n, is computed based on the Farquhar model [*Farquhar et al.*, 1980] for C$_3$ plants, and the photosynthesis scheme of *Collatz et al.* [1992] for C$_4$ plants. Overall, A_n (μmol CO$_2$ m^{-2} s^{-1}) is represented by

$$A_n = \min(A_c, A_j, A_p) - R_d \tag{2}$$

30   where A_c is the Rubisco (RuBP carboxylase/oxygenase)-limited photosynthesis rate, A_j is the RuBP-limited photosynthesis rate, A_p is the product-limited photosynthesis rate, and R_d is the dark respiration rate, all in the same unit as A_n. The

photosynthesis rate is dependent on intercellular CO_2 concentration (c_i), which is in turn dependent on g_s, c_s, and ambient CO_2 concentration (c_a) through the diffusive flux equations. A_n and g_s are therefore strongly coupled and at every model time step a unique solution for A_n and g_s is found by numerical iterations until c_i converges.

2.2 Scheme for ozone damage on vegetation

5   In the default configuration, CLM calculates stomatal conductance, which controls both water and carbon fluxes, tightly coupled to photosynthesis as mentioned above. Ozone-mediated impacts on vegetation are not included. Several land models have incorporated ozone damage by directly modifying photosynthesis using an empirical ozone flux-based factor, which in turn affects stomatal conductance [*Sitch et al.*, 2007; *Yue and Unger*, 2014]. *Lombardozzi et al.* [2012] showed that modifying photosynthesis and stomatal conductance independently using different ozone impact factors can improve model

10   simulations of vegetation responses to ozone exposure, especially with respect to hydrometeorological variables. In this study, we implement the ozone damage scheme of *Lombardozzi et al.* [2015], which modifies the initial net photosynthesis rate (A_n) and stomatal conductance (g_s) calculated by the Farquhar-Ball-Berry model (described above) independently using two ozone damage factors, F_p and F_c, which are multiplied to A_n and g_s, respectively. These two factors are calculated from the cumulative uptake of ozone (CUO), which integrates the ozone flux through leaf stomata over the growing season or leaf lifetime:

$$CUO = 10^{-6} \sum \frac{[O_3]}{k_{O_3} r_s + r_a} \Delta t \tag{3}$$

where $[O_3]$ is the surface ozone concentration (nmol m^{-3}), $k_{O_3} = 1.67$ is the ratio of leaf resistance to ozone to leaf resistance to water, r_s here is the leaf-level stomatal resistance, r_a is the aerodynamic and boundary layer resistance between leaf surface and reference level [*Sitch et al.*, 2007], and $\Delta t = 30$ min is the given model time step. CUO is only accumulated when LAI is above a minimum value of 0.5 [*Lombardozzi et al.*, 2012] and ozone flux is larger than a critical threshold of 0.8 nmol O_3 m^{-2}

20   s^{-1} to account for the compensating ability of plants to detoxify ozone. The two ozone damage factors are calculated as a linear function of CUO as:

$$F_p = a_p \times CUO + b_p \tag{4}$$
$$F_c = a_c \times CUO + b_c \tag{5}$$

where a_p, b_p, a_c and b_c are empirical slopes and intercepts (Table 1). There are 15 PFTs (*Supplement* Table S1) plus bare ground

25   in the vegetation composition of CLM4.5 [*Oleson et al.*, 2013], but as Table 1 shows, the experimental effects of ozone differ among three more general plant groups: broadleaf trees, needleleaf trees, and grasses and crops. We therefore lump CLM4.5 PFTs into the three plant groups: "broadleaf" to include all broadleaf tree and broadleaf shrub PFTs, "needleleaf" to include all needleleaf tree and shrub PFTs, and "grasses and crops" to include C_3 and C_4 grasses and C_3 unmanaged rainfed crops.

30

Table 1: Slopes (per mmol m^{-2}) and intercepts (unitless) used in Eq. (4) and Eq. (5) to relate cumulative uptake of ozone (CUO) to the ozone damage factors applied to the net photosynthesis rate and stomatal conductance, following _Lombardozzi et al._ [2015]. Values for "average" sensitivity (as opposed to "high" and "low" sensitivity) are used in this study.

	Photosynthesis		Conductance	
	Slope, a_p	Intercept, b_p	Slope, a_c	Intercept, b_c
Broadleaf	0	0.8752	0	0.9125
Needleleaf	0	0.839	0.0048	0.7823
Grasses and crops	-0.0009	0.8021	0	0.7511

2.3 Description for GEOS-Chem chemical transport model

We use the GEOS-Chem global 3-D chemical transport model version 10-01 (geos-chem.org) with fully coupled O_3-NO_x-hydrocarbon-aerosol chemical mechanism for atmospheric chemistry simulations, driven by assimilated meteorological fields from the Goddard Earth Observing System (GEOS-5) produced by the NASA Global Modeling and Assimilation Office (GMAO), with a horizontal resolution of 2° latitude by 2.5° longitude and 47 vertical layers. GEOS-Chem has been extensively used in ozone simulations and evaluated with in situ and satellite observations in previous studies, both on a global scale [e.g., _Liu et al._, 2006; _Zhang et al._, 2010] and a regional scale [e.g., _Wang et al._, 2009; _Wang et al._, 2011]. Anthropogenic emissions of NO_x, CO, sulfur dioxide (SO_2) and ammonia (NH_3) are from the EDGAR v4.2 (Emissions Database for Global Atmospheric Research) seasonal global base emission inventory for the years 1970–2008. Anthropogenic VOC emissions are from the RETRO (REanalysis of the TROpospheric chemical composition) monthly global inventory for year 2000. Biomass burning emissions are from the year-specific GFED4 (Global Fire Emissions Dataset) dataset.

In GEOS-Chem, LAI affects surface ozone mainly through three channels: biogenic VOC emissions, dry deposition, and soil NO_x emission. Biogenic emissions are calculated within GEOS-Chem by the Model of Emissions of Gasses and Aerosols from Nature (MEGAN v2.1) [_Guenther et al._, 2012]. The emission of a given VOC species is based on a baseline emission factor modulated by a series of activity factors accounting for variations in light, temperature, leaf age, soil moisture, LAI, and CO_2 inhibition. Dry deposition is computed by the resistance scheme of _Wesely_ [1989], whereby dry deposition velocity is the inverse of r_a, sublayer resistance (r_b) and bulk surface resistance (r_c) added in series. The term r_c accounts for a combination of resistances from vegetation (including stomatal resistance), lower canopy and ground, which have specific values for 11 different land types. Soil NO_x emission is based on the scheme of _Hudman et al._ [2012], and further modulated by a reduction factor to account for within-canopy NO_x deposition [_Jacob and Bakwin_, 1991].

Different modules in GEOS-Chem and CLM4.5 have traditionally used a variety of land type and PFT classification schemes. To harmonize between them, we use the land cover harmonization module recently developed by _Geddes et al._ [2016], which classifies vegetation into the same 15 PFTs as CLM4.5 (Table S1) in GEOS-Chem. Emission factors and

fractional coverages for those PFTs related to biogenic VOC emissions are mapped and regridded at model initialization. The 15 PFTs are also remapped to the 24 biomes [*Steinkamp and Lawrence*, 2011] for the soil NO$_x$ module according to their types and locations, and to the 11 land types used in the dry deposition module. Original monthly mean LAI input in GEOS-Chem derived from the Moderate Resolution Imaging Spectroradiometer (MODIS) satellite instrument at a grid-level resolution of

5   0.5°×0.5° is replaced by monthly PFT-level LAI from default CLM land surface data of the present day (year 2000), which is in turn derived from the grid-level MODIS LAI using the deaggregation methods of *Lawrence and Chase* [2007].

2.4 Model experiments to determine ozone-LAI relationship

We implement the ozone damage scheme described above into CLM4.5-BGC and conduct 11 simulations under prescribed constant ozone levels from 0 ppb to 100 ppb with an interval of 10 ppb, where the simulation with 0 ppb ozone is

10   treated as the control case (CTR) without ozone damage on vegetation. All simulations are run with initial conditions for year 2000 (which have themselves been obtained from a spin-up simulation starting from no vegetation for more than 1000 years, driven by prescribed year-2000 meteorology) for a total of 80 years. We find that vegetation structure reaches a steady state with no further temporal trends in the monthly mean values roughly after 20-40 years of simulations depending on the prescribed ozone level and PFT. Monthly mean PFT-level one-sided exposed LAI (ELAI) averaged over the last 15 simulation

15   years is extracted as the steady-state solution to be compared with the control case. Aggregate, grid-level LAI, i.e., the fraction-weighted sum over all PFTs, is also calculated.

To quantify ozone damage on vegetation structure, we define a PFT-level ozone impact factor, γ, to represent the relative change of monthly mean LAI between the case with a given ozone concentration and the control case. The PFT-level γ factors are directly calculated as:

20   $$\gamma_{\text{raw}} = \frac{\text{LAI}_{[O_3]}}{\text{LAI}_{\text{CTR}}} \qquad (7)$$

where γ_{raw} is a spatially and monthly varying ozone impact factor dependent on ozone concentration directly from the CLM simulations, LAI$_{[O_3]}$ is the simulated steady-state monthly ELAI at a given ozone concentration, and LAI$_{\text{CTR}}$ is the original monthly ELAI in the control case with no ozone damage. We find that monthly γ_{raw} (both PFT-level and grid-level) for a given location generally decreases as ozone concentration increases, but its incremental decrease for the same ozone increase

25   becomes smaller at higher ozone concentrations (Fig. 1) because of the progressive closure of stomata as represented by the ozone damage scheme. When the stomatal conductance is small enough to limit ozone flux below the critical threshold, no additional damage will be caused by ozone. This restrictive effect from attenuated stomatal conductance on ozone flux prevents LAI from declining infinitely. Thus, above a certain high-enough ozone concentration, γ_{raw} generally levels off due to a relatively steady LAI$_{[O_3]}$ in the majority of land grid cells worldwide. In some places especially in grasslands and semiarid

30   regions, however, γ_{raw} increases with ozone level but its incremental increase for the same ozone increase also declines and then levels off at higher ozone concentrations.
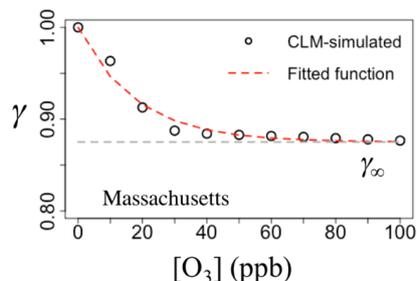
Figure 1: Relationship between the ozone impact factor, γ, for relative LAI changes in Eq. (7) and surface ozone concentration in summer (JJA), using the grid cell covering Massachusetts as an example. Black circles refer to γ_{raw} directly calculated from CLM simulated results, and the red dashed line refers to γ_{opt} in Eq. (8) that is obtained by best-fitting.

     For both kinds of ozone-LAI relationship, we can best-fit an exponential-like function to the values of CLM-simulated γ_{raw} with two optimization parameters to obtain an optimized ozone impact factor, γ_{opt}, for each model grid cell, month and PFT:

$$\gamma_{opt} = \gamma_\infty + (1 - \gamma_\infty)e^{-k[O_3]} \tag{8}$$

10 where one of the parameter to optimize, γ_∞, is essentially the "saturated" relative change in LAI at very high ozone concentrations, and k is the exponential decay factor indicating how "quickly" γ evolves with increasing ozone concentration. We find that for 90% of the grid cells/PFTs, γ_∞ is between about 0.3 and 1.5. To exclude outlying conditions where model-simulated LAI is unrealistically too sensitive to ozone (mostly in low-LAI regions at the peripheries of major forests and grasslands), we constrain the optimized γ_∞ to be between 0.3 and 1.5. We also smooth the fitted values by replacing them with

15 mean values of their surrounding grid cells if the ratio of fitted sum of squares to total sum of squares in that grid cell falls below 0.25 (i.e., if the fitted curve explains less than 25% of the variability of the simulated results). The fitting is done for both PFT-level and grid-level data, and for the vast majority of PFTs and grid cells the fitted to total sum of squares ratio is above 0.25, demonstrating the robustness of Eq. (8) as the fitting and parameterization function to be implemented in GESO-Chem (or any other CTM or climate model). The maps for fitted γ_∞ and k for different PFTs are shown in Figs. S1-2 in the

20 supplement. The global median values of annually averaged $(\gamma_\infty - 1) \times 100\%$ for different PFTs range between −19% (for needleleaf evergreen boreal trees) to +5.0% (for broadleaf deciduous temperate shrubs), and are negative for most PFTs, indicating a general decline of LAI at very high ozone levels.

2.5 GEOS-Chem experiments with ozone-vegetation coupling

We implement the parameterization equation, Eq. (8) in GEOS-Chem, and conduct three GEOS-Chem experiments (Table 2): 1) *[Intact LAI]*, a control case with monthly prescribed intact potential LAI that is unaffected by ozone; 2) *[Affected LAI]*, an experimental case with LAI being updated continuously and evolving with ozone concentration; and 3)

5 *[Intact_NoAnth]*, a case with intact potential LAI but without anthropogenic emissions, to examine the strength of ozone feedback (see Sect. 6). We run the above three cases first using 2009 to 2012 meteorology as spin-up and then loop over 2012 meteorology for three simulation years to reach a quasi-steady state for ozone air quality representative of current-day conditions. The detailed implementation algorithm for each simulation is discussed below.

10 **Table 2: GEOS-Chem experiments to investigate the effect of synchronous ozone-vegetation coupling.**

Name	Description
[Intact LAI]	GEOS-Chem simulation run with monthly intact potential LAI unaffected by ozone
[Affected LAI]	GEOS-Chem simulation run with continuously-updated LAI affected by ozone month by month
[Intact_NoAnth]	GEOS-Chem simulation run with monthly intact potential LAI unaffected by ozone and with no anthropogenic emissions of ozone precursors

For the *[Intact LAI]* case, we first derive an intact, potential LAI that should represent the maximum LAI possible if there is no ozone damage in reality, which is taken as the baseline case for investigating the effect of ozone-LAI coupling. This potential LAI is used as the initial condition to drive the GEOS-Chem simulations. The potential LAI is derived using the

15 current LAI and optimal γ_{opt} factor:

$$LAI_{pot} = \frac{LAI_{MOD}}{\gamma_{opt}} \qquad (9)$$

LAI_{MOD} here is the monthly mean PFT-level LAI from default CLM land cover for the present day originally derived from grid-level MODIS LAI. The optimal γ_{opt} is calculated using Eq. (8) from the monthly mean ozone concentrations averaged over year 2005-2008 to represent a present-day norm on which our model experiments are based.

20 For the *[Affected LAI]* case, PFT-level LAI input of each simulated month is adjusted and evolves dynamically with γ_{opt} based on the ozone concentration of the previous month. Specifically, monthly mean ozone concentration of the previous month is read in the first time step of the current simulation month and used to calculate γ_{opt} for every PFT in each grid cell, which is then multiplied to the intact potential LAI to derive a new ozone-affected LAI (LAI_{O3}) input for the current simulation month:

$$LAI_{O_3} = \gamma_{opt}\, LAI_{pot} \tag{10}$$

This manner of implementation essentially enables dynamic coevolution of LAI and ozone month by month, and assumes LAI responds to fluctuations in ozone levels on a on a monthly timescale.

Such a monthly to intraseasonal timescale for ozone-LAI coupling may not be long enough for plants to fully respond to large fluctuations of ozone concentration. As described in Sect. 2.4, when ozone is incidentally increased from zero to a prescribed level, LAI typically responds and stabilizes over about two decades. As such, is it justifiable to use the relationship between monthly mean ozone and LAI, which have reached a long-term quasi-steady state in CLM, as the basis for parameterization? We first note that, in reality, observed ozone and LAI have likely been through an extended period of coevolution and are likely coupled in a manner resembling in a quasi-steady state, albeit with seasonal fluctuations and some long-term trends. Also, the month-to-month variations in ozone concentration are typically much smaller than an incidental jump between zero and a prescribed level. We thus assume that the "steady-state response" for ozone-LAI relationship is reasonably robust to represent month-to-month variations in LAI (superimposed on the seasonality of the intact LAI). This assumption is further tested by driving CLM with hourly varying GEOS-Chem ozone fields in an asynchronously coupled experiment until LAI reaches a quasi-steady state, which will be discussed in Sect. 5.

All simulations use the same prescribed meteorological fields and PFT fractional coverage. Output variables for boreal summer (June, July and August, or JJA), boreal winter (December, January and February, or DJF), and the whole year are extracted for analysis and comparison; in the rest of this paper we will focus on boreal summer results at quasi-steady state, because this is when high ozone concentrations overlap to the greatest extent with the growing season of the majority of land plants in major populated regions at midlatitudes. Equivalent results for boreal winter and the whole year are included in the supplement and discussed briefly in the main text.

3 Impact of ozone exposure on leaf area index

We first calculate 2012 JJA mean total LAI by summing over all PFT-level LAI values weighted by the respective PFT fractional coverage, and compare the grid-level LAI_{O3} with LAI_{pot} to examine the impacts of synchronous ozone-vegetation coupling on LAI. Figure 2a shows the distribution of summertime ozone-affected LAI with a maximum value of 5.5 in Amazonia. The spatial pattern of intact, potential LAI (*Supplement* Fig. S3a) is very similar to that of affected LAI, but the magnitude is higher almost everywhere globally. The differences between these two sets of summertime LAI (*[Affected LAI] – [Intact LAI]*) are shown in Fig. 2b (the corresponding percentage changes are shown in Fig. S3b). Due to synchronous ozone-vegetation coupling on a monthly timescale, LAI values generally decline in most of the vegetated regions, and LAI experiences the greatest reduction of up to 2.6 in heavily forested regions including equatorial Asia and southeastern China. There are a few grid cells showing an opposite effect with a slight LAI increase located at the border of vegetated areas, and the possible reasons include "self-healing" effect of vegetation under moderate ozone exposure (e.g., higher water-use efficiency and increased carbon allocation to leaves) to compensate for the photosynthetic damage [*Sadiq et al.*, 2017], as well

as numerical outliers due to LAI fluctuations in low-LAI regions. Since the LAI increase in those grid cells is relatively small compared with the magnitude of LAI reduction, and almost always occurs in low-LAI or marginal areas between vegetated and non-vegetated regions, the overall impacts of those grid cells are deemed negligible.
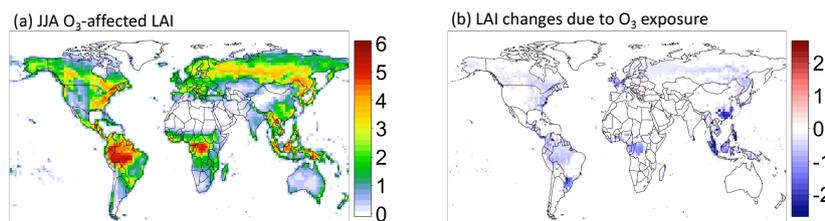
Figure 2: (a) Simulated leaf area index (LAI) affected by long-term ozone exposure in summer (JJA mean) in GEOS-Chem, and (b) differences between ozone-affected LAI in (a) and intact, potential LAI unaffected by ozone, i.e., *[Affected LAI] – [Intact LAI]*.

We also plot the PFT-level LAI changes between *[Affected LAI]* and *[Intact LAI]* case (Fig. S4), and find that total

10 LAI changes in different places are mainly caused by the dominant local PFTs: in tropical regions such as Amazonia, part of central Africa (mostly in Gabon and Congo) and equatorial Asia, the LAI changes are mainly ascribed to tropical broadleaf evergreen trees; whereas in high-latitude regions, boreal needleleaf evergreen trees play the dominant role in the LAI changes. We also find a large contribution from C_3 and C_4 grasses and rainfed crops in total LAI reduction in several subtropical and tropical regions such as southeastern China, southern Brazil, part of western Europe, and maritime Southeast Asia. This is

15 likely because of the higher sensitivity of grasses and crops to ozone exposure compared with other plant groups in this ozone damage scheme (see Table 1), and the general overestimation of grass and crop LAI in CLM, which is also documented in other studies [*Chen et al.*, 2015; *Williams et al.*, 2016].

4 Impact of synchronous ozone-vegetation coupling on surface ozone

20 Summertime (JJA) global ozone concentrations and changes due to synchronous ozone-LAI coupling are shown in Fig. 3. Figure 3a shows the JJA mean surface ozone field in the *[Affected LAI]* case, with a global average ozone concentration of 28 ppb and highest value of 75 ppb in central Africa. Figure 3b shows the differences in ozone concentration between the *[Affected LAI]* and *[Intact LAI]* case (see percentage changes in Fig. S5). With LAI being dynamically influenced by ozone in the *[Affected LAI]* case, simulated ozone concentration is generally higher in most vegetated areas such as the tropics, eastern

25 North America, and southern China by up to 3 ppb (~10%), reflecting a significant positive feedback arising from ozone-LAI coupling. The spatial patterns of both the absolute and percentage changes in simulated ozone on the continents generally match that of LAI changes due to ozone exposure (Fig. 2b), whereas ozone concentrations over the oceanic and desert areas

also increase, which is likely due to the remote transport of ozone and NO$_x$ reservoir species from high-ozone areas. We also find a slight ozone reduction in north China within 1.8 ppb and in central North America within 0.8 ppb; these places experience moderate ozone exposure in summer but relatively little LAI changes. Such a reduction is driven by reduced transport of VOCs as well as organic nitrate formed from VOC-NO$_x$ reactions following reduced LAI elsewhere in more vegetated regions

5   [*Hollaway et al.*, 2017].
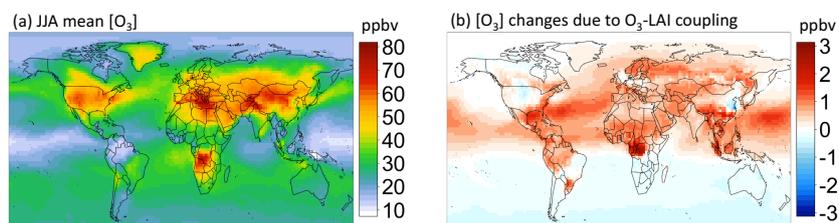
Figure 3: (a) Surface ozone concentration with ozone-affected leaf area index (LAI) in boreal summer (JJA mean) from the *[Affected LAI]* case; and (b) differences in JJA ozone concentration between the *[Affected LAI]* and *[Intact LAI]* case (i.e., *[Affected LAI]* – *[Intact LAI]*).

We further investigate the possible pathways contributing to the above simulated ozone changes. Figure 4a shows the JJA ozone dry deposition velocity (v_d, cm s^{-1}) in the *[Affected LAI]* case, which mirrors the global LAI distribution, reflecting leaf stomatal uptake of ozone. Its absolute changes compared with the *[Intact LAI]* case are shown in Fig. 4b (corresponding

15   percentage changes are shown in Fig. S6), which indicates that regions with a large LAI reduction also have a large decline in ozone dry deposition velocity. The spatial pattern of such a decline is broadly consistent with that of the ozone reduction, suggesting that reduced dry deposition velocity due to ozone-induced LAI decline is an important factor for the higher ozone shown in Fig. 3b.
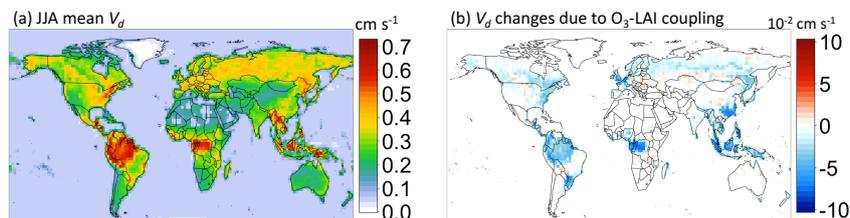
Figure 4: (a) Ozone dry deposition velocity (v_d) in summer (JJA mean) from the *[Affected LAI]* case; and (b) differences in ozone dry deposition velocity between the *[Affected LAI]* and *[Intact LAI]* case (i.e., *[Affected LAI]* – *[Intact LAI]*).

Global isoprene emission rate (nmol m^{-2} s^{-1}) in summer in the *[Affected LAI]* case and its differences from the *[Intact LAI]* case are shown in Fig. 5a and 5b, respectively (percentage changes are shown in Fig. S7). Isoprene, which is one of the most important biogenic VOCs determining ambient ozone, shows a general decline globally, mostly reflecting the strong

5   association between isoprene emission and LAI. Unlike LAI reduction, however, the greatest absolute reduction for isoprene emission occurs in central Africa rather than throughout the entire tropical regions, mainly because of the high baseline isoprene emission in this region, so that a similar perturbation in LAI may induce a particularly large change in isoprene emission.
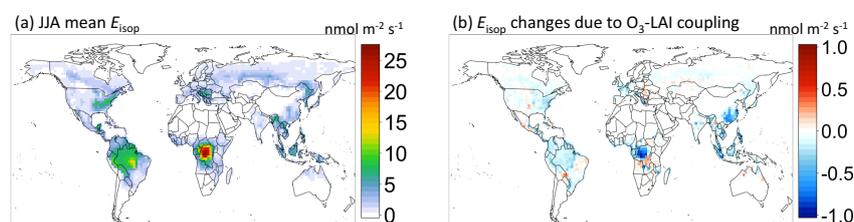
Figure 5: (a) Isoprene emission rate (E_{isop}) in summer (JJA mean) from the *[Affected LAI]* case; and (b) differences in isoprene emission rate between the *[Affected LAI]* and *[Intact LAI]* case (i.e., *[Affected LAI]* – *[Intact LAI]*).

Isoprene plays opposite roles in ozone changes depending on the ambient NO$_x$ level. Figure 6 shows the summertime

15   surface NO$_x$ concentration as well as its changes between the *[Affected LAI]* and *[Intact LAI]* case. In the relatively high-NO$_x$ regions at northern midlatitudes (over North America, Europe and East Asia), ozone enhancement from ozone-LAI coupling is relatively small compared with the subtropical and tropical regions (Fig. 3b). This is mostly due to the compensation between the effects of reduced dry deposition, which increases ozone, and reduced isoprene emission, which decreases ozone. In Europe and northern China, in particular, ozone-LAI coupling enhances NO$_x$ level due to reduced sequestration by biogenic VOCs

20   (Fig. 6b), which further limits ozone production due to more sequestration of OH by NO$_x$ (shown in Fig. S8) and thus less efficient cycling of HO$_x$ radicals. On the other hand, in the subtropical and tropical regions where isoprene emission is high (Fig. 5a) and NO$_x$ level is relatively low (Fig. 6a), reduced dry deposition (Fig. 4b) and reduced isoprene emission (Fig. 5b) add together to enhance ozone concentrations.
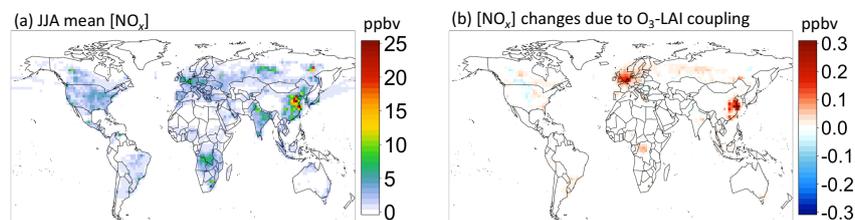
Figure 6: (a) Surface NO$_x$ concentration in summer (JJA mean) from the *[Affected LAI]* case; and (b) differences in NO$_x$ concentration between the *[Affected LAI]* and *[Intact LAI]* case (i.e., *[Affected LAI] – [Intact LAI]*).

5   We further estimate the relative contribution of reduced dry deposition vs. isoprene emission toward the simulated ozone changes under ozone-LAI coupling using the statistical model developed by *Wong et al.* [2018], which is designed to be a computationally simple assessment tool to estimate the local sensitivity of ozone to any LAI changes and attribute this sensitivity to each of the two pathways based on an array of simulated variables including ozone concentration, total NO$_x$ emission, wind speed, temperature, etc., for any vegetated locations. According to the statistical model, we find that ozone is

10 significantly enhanced globally when driven only by reduced ozone dry deposition (Fig. 7a), and mildly reduced when driven only by isoprene emission (Fig. 7b). The possible total ozone changes via both pathways combined (Fig. 7c) broadly match the pattern of ozone changes on the continents directly simulated by GEOS-Chem (Fig. 3b). The statistical model suggests that reduced ozone dry deposition plays a more dominant role in the total ozone changes, and reduced biogenic isoprene emission generally causes a decline in ozone that partially offsets the effect of reduced dry deposition especially in northern midlatitude

15 high-NO$_x$ regions where ozone sensitivity to isoprene emission is stronger than in tropical low-NO$_x$ regions. In general, anthropogenic NO$_x$ emission and baseline LAI are the most important factors determining which of dry deposition vs. biogenic emissions is the dominant pathway accounting for local ozone responses to LAI changes.
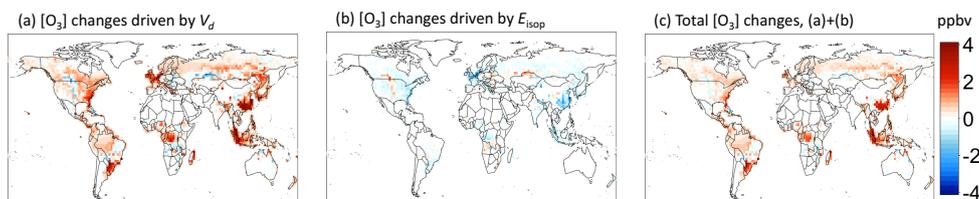
20 **Figure 7: Attrition of simulated ozone changes to (a) changes in dry deposition only; (b) changes in biogenic isoprene emission only; and (c) changes in both dry deposition and isoprene emission combined, based on the statistical model developed by *Wong et al.* [2018].**

Equivalent plots of Fig. 3 but for boreal wintertime (DJF) mean and annual mean ozone are shown in Fig. S5. Annual ozone changes due to ozone-LAI coupling are broadly consistent with that for JJA mean, albeit with weaker negative feedbacks and more spatially dispersed positive feedbacks. The wintertime ozone enhancements in the Northern Hemisphere are generally much stronger and more widespread than those in summer, mostly due to the smaller importance of isoprene emission in counteracting the deposition-mediated positive feedbacks.

5 Impacts of asynchronous ozone-vegetation coupling on surface ozone

In the above we have presented the effect of synchronous ozone-LAI coupling, whereby ozone and LAI interact dynamically "online" on a monthly timescale according to a simplified parameterization scheme, on ozone air quality. Here we perform an additional series of GEOS-Chem and CLM experiments to determine the effect of ozone-LAI coupling if the coupling is done asynchronously. The results from these experiments, in comparison with those in Sect. 4, allow us to: 1) examine the relative importance of first-order and second-order feedback effects; 2) check if driving CLM with temporally varying ozone fields would yield different results; and 3) evaluate if the "quasi-steady state response" assumption behind the ozone-LAI synchronous coupling is reasonable.

We first simulate hourly ozone concentrations using GEOS-Chem under year-2012 conditions, which are then used to drive CLM with the ozone damage scheme (Sect. 2.2) for at least 20 simulation years until a quasi-steady state is reached. The resulting relative changes in monthly LAI at PFT levels due to ozone damage are then multiplied by the intact potential LAI, and fed into GEOS-Chem to simulate hourly ozone concentrations again, which are then fed back to CLM to estimate the "new" steady-state LAI changes, finishing one cycle. In theory, the feedback cycles should carry on until relative LAI changes and ozone concentrations come into equilibrium with each other. In practice, we find that the second-order LAI changes after one cycle of asynchronous coupling are much smaller than the first-order changes and yield only negligible further changes in ozone concentrations, suggesting that the first-order effect has already encapsulated most of the coupling effect.

The asynchronous ozone-LAI coupling experiments have the same model configurations as described in Sect. 2.4 and 2.5, except that γ_{raw} in Eq. (7) is now calculated with CLM-simulated LAI driven by hourly ozone fields from the *[Intact LAI]* case, instead of constant ozone levels. We constrain γ_{raw} to be within the range of 0.3 to 1.6, which covers more than 90% of its values. In the *[Affected LAI]* case here, we replace γ_{opt} in Eq. (10) with γ_{raw} to obtain LAI_{O3}, which are then used as boundary conditions for GEOS-Chem simulation.

The differences in LAI between the *[Affected LAI]* and *[Intact LAI]* case are shown in Figs. S9 and S10. The mostly negatively relative changes in LAI here for asynchronous coupling are broadly consistent with that shown in Fig. S3 for synchronous coupling, albeit with more frequent occurrences of the sporadic LAI increases in low-LAI regions. This is expected because in the development of parameterization for synchronous ozone-LAI coupling, many of these grid cells are filtered out due to poor fitting by Eq. (8). The overall strong resemblance between the relative LAI changes in both approaches

suggests that the simplified, computationally efficient parameterization for ozone-LAI coupling on a monthly timescale (Sect. 2.4) is a reasonable idealization of the cumulative long-term steady-state responses of vegetation to temporally varying ozone levels.

Figure 8 shows the JJA mean surface ozone in the *[Affected LAI]* case and the changes from the *[Intact LAI]* case due to asynchronous ozone-LAI coupling. Simulated ozone concentrations are in the same range as that for synchronous coupling with a global average of 28 ppb and highest value of 79 ppb in central Africa. The absolute (Fig. 8b) and relative (Fig. S11) differences in ozone concentrations between the *[Affected LAI]* and *[Intact LAI]* case are broadly consistently with that for synchronous ozone-LAI coupling (Fig. 3b and Fig. S5), but are generally more localized. Similar to the synchronously coupled case, simulated ozone concentrations are higher especially in the tropics, eastern North America, Europe, and southern China by up to 3 ppb, indicating a strong positive feedback due to ozone-LAI interactions. The same figures as Figs. 4-6 but for asynchronous coupling are included in the supplement (Figs. S12-S16), also showing show broadly consistent patterns. Most of the bigger differences occur in low-LAI regions which are more prone to idiosyncratic model (CLM) behaviors and numerical outliers especially in the asynchronously coupled cases where such peculiarities are not smoothed out.
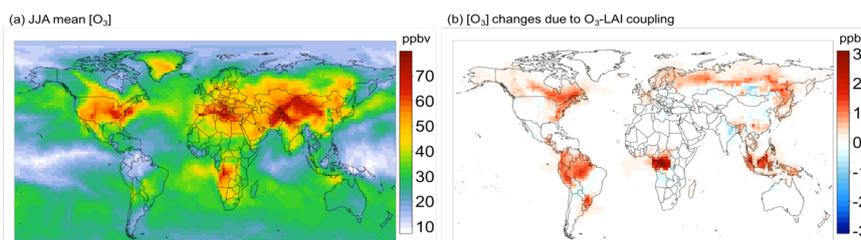
Figure 8: (a) Surface ozone concentration with ozone-affected leaf area index (LAI) in summer (JJA mean) from the *[Affected LAI]* case for asynchronous ozone-LAI coupling; and (b) differences in JJA ozone concentration between the *[Affected LAI]* and *[Intact LAI]* case (i.e., *[Affected LAI]* – *[Intact LAI]*).

6 Ozone feedback factor

Climate feedback factor has been widely used in climate studies to indicate how the initial, "direct" surface temperature change driven by a given radiative forcing can be dampened or amplified by internal feedback mechanisms in the climate system [*IPCC*, 2013]. Here we analogously develop the concept of ozone feedback factor, f, which can be used to indicate how an initial ozone change ($\Delta[O_3]_i$) driven by anthropogenic forcing of precursor emissions (mostly NO_x and VOCs) can be amplified or dampened by various processes within the earth system (e.g., ozone-vegetation coupling) to arrive at a final ozone change ($\Delta[O_3]_f$):

$$\Delta[O_3]_f = \frac{\Delta[O_3]_i}{1-f} \tag{11}$$

Here, we conduct a simulation, *[Intact_NoAnth]*, in GEOS-Chem with the same settings as the *[Intact LAI]* case (for synchronous coupling) but with all anthropogenic emissions turned off (Table 3). Therefore, the differences between this case and *[Intact LAI]* necessarily represent the effect of anthropogenic forcing (mostly by fossil fuel combustion) on surface ozone changes without any ozone-LAI coupling effect, whereas that the difference between this case and *[Affected LAI]* represents

5   the final effect with (synchronous) ozone-LAI coupling and feedback. That is, in Eq. (11), $\Delta[O_3]_i$ and $\Delta[O_3]_f$ are the differences in ozone concentrations, *[Intact LAI]* − *[Intact_NoAnth]* and *[Affected LAI]* − *[Intact_NoAnth]*, respectively. Thus, *f* here reflects the strength and sign of feedback effect from ozone-vegetation coupling on ozone concentration itself, and a value of $f < 0$ represents a negative feedback whereby ozone changes are dampened by ozone-vegetation interactions, and $0 < f < 1$ represents a positive feedback whereby ozone changes are amplified by ozone-vegetation interactions.

10   The summertime *f* factor for ozone-LAI coupling based on GEOS-Chem simulations is shown in Fig. 9, where the red areas indicate a positive feedback on ozone concentration after incorporating ozone-LAI coupling and blue areas indicate a negative feedback. We find a significant positive feedback signal in central Africa and the Amazon region, which also experience a relatively large reduction in ozone dry deposition and isoprene emission due to ozone-LAI coupling. The strong positive feedback over these tropical forest regions is mostly caused by the combined effects of reduced dry deposition and

15   reduced isoprene emission (to a lesser extent) in a low-NO_x environment, which act in the same direction to increase surface ozone. The negative feedback in many remote regions with low or no LAI, e.g., central North America and most of the Southern Hemisphere, is mostly a result of reduced transport of NO_x reservoir species formed from reactions of NO_x and biogenic VOCs. In contrast, in high-population, high-NO_x regions including the eastern US, Europe and eastern China, the relatively weak positive feedback and even negative feedback (in North China) mostly reflect the compensating effects of reduced isoprene

20   emission (which reduces ozone in high-NO_x regime) and reduced dry deposition (which enhances ozone).
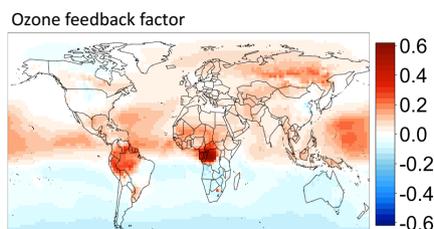
Figure 9: Ozone feedback factor distribution in summer due to ozone-LAI coupling.

25   Generally, ozone feedback factor of $f > 0$ (positive feedback) occurs in most heavily vegetated areas with low NO_x levels. Distinct ozone positive feedbacks in the tropics indicate a significant effect from ozone-LAI coupling, which can have important ramifications for future ozone projections. In major populated regions at northern midlatitudes, the relatively weak

feedback effect is not a result of the insignificance of every individual pathway, but rather reflects compensating effect between several important pathways.

7 Conclusions and discussion

5   In this study, we develop a parameterized function for an ozone impact factor on LAI by conducting various land surface-biogeochemical model simulations using CLM with an empirical scheme of ozone damage on vegetation to represent the impact of long-term ozone exposure on monthly mean LAI. We then conduct various sets of atmospheric chemical transport simulations using GEOS-Chem driven by present-day meteorological conditions and PFT fractional coverage under various configurations: with and without the parameterized ozone-LAI relationship (ozone-affected LAI vs. intact, potential LAI), with and without anthropogenic emissions, and with synchronous vs. asynchronous ozone-LAI coupling. Such configurations allow us to investigate the impacts of ozone-LAI coupling on simulated ozone air quality and vegetation health, as well as the sign and strength of vegetation-mediated ozone feedback, which can either dampen or amplify the effect of anthropogenic emissions on tropospheric ozone levels.

        Generally, ozone damage causes a global LAI reduction for most PFTs under long-term ozone exposure. Compared with the hypothetical intact LAI that is unaffected by ozone, the reduction in PFT-weighted LAI can be as high as 2.6 (percentage reduction up to 50%) in high-LAI regions. Only a few studies of ozone-vegetation interactions have considered this important vegetation structural parameter in coupled model simulations [e.g., *Yue and Unger*, 2014; *Sadiq et al.*, 2017]. The magnitude of simulated LAI changes in this study is quite different from that of *Sadiq et al.* [2017], who used the same ozone damage scheme from *Lombardozzi et al.* [2015] but in a fully coupled land-atmosphere model (CLM4CN-CAM4-Chem) where meteorological variables are also modified dynamically by both stomatal and LAI changes. They found a relatively irregular pattern of summertime LAI changes and the magnitude is generally small (within 5%), likely due to more favorable meteorological conditions triggered by stomatal changes that partly counteract ozone-induced photosynthetic damage (e.g., more convective precipitation and enhanced soil moisture in certain places where surface temperature increases).

        Incorporating the ozone-induced damage on LAI in the GEOS-Chem chemical transport model, we find an ozone feedback of −1.8 ppb to +3 ppb globally, and a corresponding ozone feedback factor of about −0.1 to +0.6. The strongest positive feedback from ozone-LAI coupling is found in tropical forests, where dry deposition plays the dominant role modulating the feedback. *Sadiq et al.* [2017] called this kind of feedback "biogeochemical" because it is effected directly through plant physiological responses and allocation to structural parts. *Sadiq et al.* [2017] also considered "biogeophysical" or "meteorological" feedback, whereby ozone-induced damage on plants causes a cascade of meteorological changes that ultimately affect ozone itself. In their study, the total ozone feedback is up to +4-6 ppb, and based on sensitivity simulations they attributed roughly half of that to biogeochemical feedback, which is consistent in both magnitude and sign with this study despite the use of different chemical transport models, although in their study stomatal changes (not considered in this study) play a larger role in the biogeochemical feedback than LAI changes. The remaining positive feedback in their study mostly

arises from biogeophysical feedback, whereby reduced stomatal conductance following ozone damage leads to less transpiration, higher vegetation temperature and thus higher isoprene emission. However, they noted that dynamically changing hydrometeorological variables and processes are not generally tuned for atmospheric chemical measurements, and may introduce large uncertainty in simulating and attributing boundary-layer ozone concentrations to various determining

5   factors.

As our ozone-LAI coupling approach is embedded within a chemical transport model driven by prescribed meteorology, the feedback effects on surface ozone in this study is purely biogeochemical, and decidedly do not include the complication arising from meteorological changes. The feedbacks are attributable to different pathways in different regions. In tropical regions such as maritime Southeast Asia, Amazonia and central Africa, the strong summertime positive ozone

10   feedback is mainly due to the ozone-induced LAI reduction and the subsequent decrease in ozone dry deposition. Reduced isoprene emission further enhances the feedback in these low-NO_x environments but is relatively minor due to the relatively lower sensitivity of ozone to isoprene emission in these regions. In contrast, in high-NO_x regions such as the eastern US, Europe and eastern China, reduced isoprene emission decreases ozone, and this counteracts with the positive feedback from dry deposition, yielding relatively small or even negative feedback effects there. Over the oceans in the Northern Hemisphere,

15   surface ozone concentration also increases in response to reduced LAI on the continents, mainly because of continental outflow. Over most of the Southern Hemisphere, there is a weak negative feedback, which is likely driven by reduced intercontinental transport of organic nitrate (as a reservoir of NO_x) formed from NO_x-VOC reactions.

Uncertainty can arise from the large variability in the ozone sensitivity of different plants, especially for tropical trees and grasses, which are modeled based on relatively insufficient data as compared with temperature ecosystems [*Lombardozzi*

20   *et al.*, 2013]. Although the current *Lombardozzi et al.* [2015] scheme classifying 15 PFTs into three plant groups is relatively robust in capturing the average plant physiological responses to ozone uptake on a global scale from across many studies, more detailed experimental and field data can potentially help us derive a more precise parameterization for different PFTs that can be particularly useful for high-resolution regional air quality simulations.

Another possible caveat comes from the timescale of plant responses to ozone. Forcing LAI input in GEOS-Chem

25   simulations to be continuously modified by the ozone impact factor γ at the beginning of every month necessarily assumes ozone-LAI coupling to occur on a monthly to intraseasonal timescale, but the parameterization of ozone-LAI relationship is based on the long-term (typically decadal) quasi-steady state. As discussed in Sect. 2.5 and Sect. 5, we deem this "steady-state response" assumption a reasonable idealization for ozone-LAI coupling even on shorter timescales, which is further buttressed by the resemblance of its simulated responses to the asynchronously coupled experiments where LAI and temporally varying

30   ozone always equilibrate with each other. We note, however, that our parameterization necessarily ignores hysteresis effect, whereby damage done at incidentally high ozone concentrations may not undergo full recovery even when ozone levels drop again.

This study focuses exclusively on ozone-LAI coupling, but the interaction between ozone and stomatal conductance has also been shown to significantly modulate ozone-vegetation feedbacks [*Sadiq et al.*, 2017]. Ozone-stomata coupling using

the same modeling framework certainly warrants further investigation. Moreover, in this study meteorological conditions are prescribed and looped over for a typical year only, and thus the potential impacts of interannual climate variability on the ozone-LAI relationships are not fully considered. For instance, the occurrence of droughts may either weaken or strengthen the coupling between plants and ozone by interfering with photosynthetic capacity and stomatal behaviors [e.g., *Wang et al.*,

5   2017]. Our findings still attest to the existence of strong ozone biogeochemical feedbacks under typical conditions, and highlight the importance of incorporating ozone-vegetation coupling into regional to global ozone air quality and ecosystem health assessment so that more realistic future projections can be made.

Data availability

10   Most of the data produced by this study and presented in the manuscript are deposited in the publicly available institutional repository, accessible via this link: http://www.cuhk.edu.hk/sci/essc/tgabi/data.html. Request for raw data or the complete set of data, or any questions regarding the data, can be directed to the principal investigator, Amos P. K. Tai (amostai@cuhk.edu.hk).

15   **Acknowledgement**

This work was supported by the Early Career Scheme (Project #: 24300614) of the Research Grants Council of Hong Kong given to the principal investigator, Amos P. K. Tai. We also thank the Information Technology Services Centre (ITSC) at The Chinese University of Hong Kong for their devotion in providing the necessary computational services for this work. Colette L. Heald acknowledges the support from the National Science Foundation (ATM-1564495) for the development of

20   land cover harmonization used in this work.

References

Ainsworth, E. A., C. R. Yendrek, S. Sitch, W. J. Collins, and L. D. Emberson: The effects of tropospheric ozone on net primary productivity and Implications for climate change, *Annu. Rev. Plant Biol.*, *63*(1), 637–661, doi:10.1146/annurev-arplant-042110-103829, 2012.

25   Anenberg, S. C., L. W. Horowitz, D. Q. Tong, and J. J. West: An estimate of the global burden of anthropogenic ozone and fine particulate matter on premature human mortality using atmospheric modeling, *Environ. Health Perspect.*, *118*(9), 1189–1195, doi:10.1289/ehp.0901220, 2010.

Ball, J. T., I. E. Woodrow, and J. A. Berry: A model predicting stomatal conductance and its contribution to the control of photosynthesis under different environmental conditions, in *Progress in Photosynthesis Research*, pp. 221–224, Springer

30   Netherlands, Dordrecht, 1987.

Bey, I., D. J. Jacob, R. M. Yantosca, J. A. Logan, B. D. Field, A. M. Fiore, Q. Li, H. Y. Liu, L. J. Mickley, and M. G. Schultz: Global modeling of tropospheric chemistry with assimilated meteorology: Model description and evaluation, *J. Geophys. Res. Atmos.*, *106*(D19), 23073–23095, doi:10.1029/2001JD000807, 2001.

Chen, M., T. J. Griffis, J. Baker, J. D. Wood, and K. Xiao: Simulating crop phenology in the Community Land Model and its impact on energy and carbon fluxes, *J. Geophys. Res. Biogeosciences*, *120*(2), 310–325, doi:10.1002/2014JG002780, 2015.

Collatz, G., M. Ribas-Carbo, and J. Berry: Coupled photosynthesis-stomatal conductance model for leaves of C_4 plants, *Aust. J. Plant Physiol.*, *19*(5), 519, doi:10.1071/PP9920519, 1992.

Collatz, G. J., J. T. Ball, C. Grivet, and J. A. Berry: Physiological and environmental regulation of stomatal conductance, photosynthesis and transpiration: a model that includes a laminar boundary layer, *Agric. For. Meteorol.*, *54*(2–4), 107–136, doi:10.1016/0168-1923(91)90002-8, 1991.

Farquhar, G. D., S. von Caemmerer, and J. A. Berry: A biochemical model of photosynthetic CO_2 assimilation in leaves of C_3 species., *Planta*, *149*(1), 78–90, doi:10.1007/BF00386231, 1980.

Geddes, J. A., C. L. Heald, S. J. Silva, and R. V. Martin: Land cover change impacts on atmospheric chemistry: Simulating projected large-scale tree mortality in the United States, *Atmos. Chem. Phys.*, *16*(4), 2323–2340, doi:10.5194/acp-16-2323-2016, 2016.

Guenther, A., T. Karl, P. Harley, C. Wiedinmyer, P. I. Palmer, and C. Geron: Estimates of global terrestrial isoprene emissions using MEGAN (Model of Emissions of Gases and Aerosols from Nature), *Atmos. Chem. Phys.*, *6*(11), 3181–3210, doi:10.5194/acp-6-3181-2006, 2006.

Guenther, A. B., X. Jiang, C. L. Heald, T. Sakulyanontvittaya, T. Duhl, L. K. Emmons, and X. Wang: The model of emissions of gases and aerosols from nature version 2.1 (MEGAN2.1): An extended and updated framework for modeling biogenic emissions, *Geosci. Model Dev.*, *5*(6), 1471–1492, doi:10.5194/gmd-5-1471-2012, 2012.

Hollaway, M. J., S. R. Arnold, W. J. Collins, G. Folberth, and A. Rap: Sensitivity of midnineteenth century tropospheric ozone to atmospheric chemistry-vegetation interactions, *J. Geophys. Res. Atmos.*, *122*(4), 2452–2473, doi:10.1002/2016JD025462, 2017.

Horowitz, L. W., A. M. Fiore, G. P. Milly, R. C. Cohen, A. Perring, P. J. Wooldridge, P. G. Hess, L. K. Emmons, and J. F. Lamarque: Observational constraints on the chemistry of isoprene nitrates over the eastern United States, *J. Geophys. Res. Atmos.*, *112*(12), doi:10.1029/2006JD007747, 2007.

Hudman, R. C., N. E. Moore, A. K. Mebust, R. V. Martin, A. R. Russell, L. C. Valin, and R. C. Cohen: Steps towards a mechanistic model of global soil nitric oxide emissions: Implementation and space based-constraints, *Atmos. Chem. Phys.*, *12*(16), 7779–7795, doi:10.5194/acp-12-7779-2012, 2012.

IPCC: Climate Change 2013: The Physical Science Basis. Contribution of Working Group I to the Fifth Assessment Report of the Intergovernmental Panel on Climate Change, *Cambridge Univ. Press. Cambridge, United Kingdom New York, USA*, 1535 pp, doi:10.1017/CBO9781107415324, 2013.

Jacob, D. J., and P. S. Bakwin: Cycling of NO$_x$ in tropical forest canopies, in *Microbial production and consumption of greenhouse gases: methane, nitrogen oxides, and halomethanes*, pp. 237–253, 1991.

Karnosky, D. F., J. M. Skelly, K. E. Percy, and A. H. Chappelka: Perspectives regarding 50 years of research on effects of tropospheric ozone air pollution on US forests, *Environ. Pollut.*, *147*(3), 489–506, doi:10.1016/j.envpol.2006.08.043, 2007.

5   Lawrence, P. J., and T. N. Chase: Representing a new MODIS consistent land surface in the Community Land Model (CLM 3.0), *J. Geophys. Res. Biogeosciences*, *112*(1), doi:10.1029/2006JG000168, 2007.

Liu, X. et al.: First directly retrieved global distribution of tropospheric column ozone from GOME: Comparison with the GEOS-CHEM model, *J. Geophys. Res. Atmos.*, *111*, D02308, doi:10.1029/2005JD006564, 2006.

Lombardozzi, D., S. Levis, G. Bonan, and J. P. Sparks: Predicting photosynthesis and transpiration responses to ozone:
10   Decoupling modeled photosynthesis and stomatal conductance, *Biogeosciences*, *9*(8), 3113–3130, doi:10.5194/bg-9-3113-2012, 2012.

Lombardozzi, D., J. P. Sparks, and G. Bonan: Integrating O$_3$ influences on terrestrial processes: photosynthetic and stomatal response data available for regional and global modeling, *Biogeosciences*, *10*(11), 6815–6831, doi:10.5194/bg-10-6815-2013, 2013.

15   Lombardozzi, D., S. Levis, G. Bonan, P. G. Hess, and J. P. Sparks: The influence of chronic ozone exposure on global carbon and water cycles, *J. Clim.*, *28*(1), 292–305, doi:10.1175/JCLI-D-14-00223.1, 2015.

Oleson, K. W. et al.: Technical Description of version 4.5 of the Community Land Model (CLM), *NCAR Tech. Note NCAR/TN-503+STR*, 420 pp, doi:10.5065/D6RR1W7M, 2013.

Oltmans, S. J. et al.: Recent tropospheric ozone changes - A pattern dominated by slow or no growth, *Atmos. Environ.*, *67*,
20   331–351, doi:10.1016/j.atmosenv.2012.10.057, 2013.

Sadiq, M., A. P. K. Tai, D. Lombardozzi, and M. Val Martin: Effects of ozone-vegetation coupling on surface ozone air quality via biogeochemical and meteorological feedbacks, *Atmos. Chem. Phys.*, *17*(4), 3055–3066, doi:10.5194/acp-17-3055-2017, 2017.

Sakalli, A., A. Cescatti, A. Dosio, and M. U. Gücel: Impacts of 2°C global warming on primary production and soil carbon
25   storage capacity at pan-European level, *Clim. Services*, *7*, 64-77. doi:10.1016/j.cliser.2017.03.006, 2017.

Sitch, S., P. M. Cox, W. J. Collins, and C. Huntingford: Indirect radiative forcing of climate change through ozone effects on the land-carbon sink, *Nature*, *448*(7155), 791–794, doi:10.1038/nature06059, 2007.

Steinkamp, J., and M. G. Lawrence: Improvement and evaluation of simulated global biogenic soil NO emissions in an AC-GCM, *Atmos. Chem. Phys.*, *11*(12), 6063–6082, doi:10.5194/acp-11-6063-2011, 2011.

30   Sun, Y., L. Gu, and R. E. Dickinson: A numerical issue in calculating the coupled carbon and water fluxes in a climate model, *J. Geophys. Res. Atmos.*, *117*(22), 1–16, doi:10.1029/2012JD018059, 2012.

Volz, A., and D. Kley: Evaluation of the Montsouris series of ozone measurements made in the nineteenth century, *Nature*, *332*(6161), 240–242, 1988.

Wang, H., D. J. Jacob, P. Le Sager, D. G. Streets, R. J. Park, A. B. Gilliland, and A. van Donkelaar: Surface ozone background in the United States: Canadian and Mexican pollution influences, *Atmos. Environ.*, *43*(6), 1310–1319, doi:10.1016/j.atmosenv.2008.11.036, 2009.

Wang, Y., J. A. Logan, and D. J. Jacob: Global simulation of tropospheric O_3-NO_x-hydrocarbon chemistry: 2. Model evaluation and global ozone budget, *J. Geophys. Res. Atmos.*, *103*(D9), 10727–10755, doi:10.1029/98JD00157, 1998.

Wang, Y., Y. Zhang, J. Hao, and M. Luo: Seasonal and spatial variability of surface ozone over China: Contributions from background and domestic pollution, *Atmos. Chem. Phys.*, *11*(7), 3511–3525, doi:10.5194/acp-11-3511-2011, 2011.

Wang, Y.-Y., Z.-H. Xie, B.-H. Jia, and Y. Yu: Improving simulation of the terrestrial carbon cycle of China in version 4.5 of the Community Land Model using a revised V_{cmax} scheme, *Atmos. Ocean. Sci. Lett.*, *8*(2), 88-94, doi:10.3878/AOSL20140090, 2015.

Wesely, M. L.: Parameterization of surface resistances to gaseous dry deposition in regional-scale numerical models, *Atmos. Environ.*, *23*(6), 1293–1304, doi:10.1016/0004-6981(89)90153-4, 1989.

Wild, O.: Modelling the global tropospheric ozone budget: exploring the variability in current models, *Atmos. Chem. Phys.*, *7*, 2643–2660, doi:10.5194/acpd-7-1995-2007, 2007.

Williams, I. N., Y. Lu, L. M. Kueppers, W. J. Riley, S. C. Biraud, J. E. Bagley, and M. S. Torn: Land-atmosphere coupling and climate prediction over the U.S. Southern Great Plains, *J. Geophys. Res. Atmos.*, *121*, 12,125-12,144, doi:10.1002/2016JD025223, 2016.

Wang, Y., Y. Xie, W. Dong, Y. Ming, J. Wang, and L. Shen: Adverse effects of increasing drought on air quality via natural processes, *Atmos. Chem. Phys.*, 17, 12827-12843, doi:10.5194/acp-17-12827-2017, 2017.

Wong, A. Y. H., A. P. K. Tai, and Y.-Y. Ip: Attribution and statistical parameterization of the sensitivity of surface ozone to changes in leaf area index based on a chemical transport model, *J. Geophys. Res.-Atmos.*, 123, 1883-1898, doi:10.1002/2017JD027311, 2018.

Yue, X., and N. Unger: Ozone vegetation damage effects on gross primary productivity in the United States, *Atmos. Chem. Phys.*, *14*(17), 9137–9153, doi:10.5194/acp-14-9137-2014, 2014.

Yue, X., and N. Unger: The Yale Interactive terrestrial Biosphere model version 1.0: Description, evaluation and implementation into NASA GISS ModelE2, *Geosci. Model Dev.*, *8*(8), 2399–2417, doi:10.5194/gmd-8-2399-2015, 2015.

Zhang, L., D. J. Jacob, X. Liu, J. A. Logan, K. Chance, A. Eldering, and B. R. Bojkov: Intercomparison methods for satellite measurements of atmospheric composition: Application to tropospheric ozone from TES and OMI, *Atmos. Chem. Phys.*, *10*(10), 4725–4739, doi:10.5194/acp-10-4725-2010, 2010.